A NURBS-BASED TECHNIQUE FOR THE SEGMENTATION OF MEDICAL IMAGES

Ravinda G.N. Meegama and Jagath C. Rajapakse
School of Computer Engineering, Nanyang Technological University
Nanyang Avenue, Singapore 639798
e-mail: gayan@sentosa.sas.ntu.edu.sg, asjagath@ntu.edu.sg

Abstract

Extracting the human brain from magnetic resonance head scans is difficult because of its highly convoluted and nonuniform geometry. A technique based on Non-Uniform Rational B-Splines (NURBS) and energy minimising deformable models to extract the brain surface accurately from MR head scans is presented. The weighting parameter that comes with the NURBS definition is explored to attract the surface into the regions showing high curvature. The weight at each control point is adjusted automatically according to the curvature properties of the evolving surface. This process facilitates a deformable surface with increased local flexibility that adapts to complex geometrical features of the brain. The results show that the proposed model is capable of capturing the correct brain surface with a higher accuracy than the existing techniques.

1. Introduction

Magnetic Resonance (MR) head scans indicate the skull, subarachnoid fluid and other anatomical structures that hamper the visibility of the brain surface. Therefore, in order to carry out an accurate morphometry in neurological studies, the brain has to be separated from these external structures. Such a segmentation routine is of immense assistance for various clinical studies because the surface patterns of the brain are considered to be natural pathways on the subarachnoid system that can be used to access pathological structures within the brain [10].

Several researchers have investigated the problem of modeling the brain surface using deformable models [1, 7, 14, 15, 17]. Our research, an extension to "Dynamic NURBS" [13], is motivated by the limitations found in the previous techniques that require manual initialisation, user interaction during deformation, poor local shape control and redundant points to capture the brain surface accurately. The approach presented in this paper emphasises on developing a surface model to segment the brain accurately from MR head scans with minimum user intervention. The main reason for the selection of a NURBS surface for our algorithm is its inherent locally adaptable features [12]. In other words, a movement of a particular control point (or a change in the weight of a control point) alters the shape of the surface segment lying immediately close to that point. This is in sharp contrast to other deformable models based on irregular mesh configurations where such changes tend to propagate globally on the surface [1, 8, 9, 15].

The proposed method consists of two stages: First, we obtain the brain matter using an approximate segmentation routine. Manual initialisation is avoided by taking the output image from this procedure to construct the initial NURBS surface that is positioned close to the actual boundary of the brain matter. The second stage involves deforming the above NURBS surface according to an energy minimisation algorithm and also, modifying the weight associated with each control point automatically depending on the curvature properties of the evolving surface. This weight modification forces parts of the surface near sulci (grooves on the brain surface) to attract towards the cavities without having to duplicate the control points near such regions. By using a NURBS-based deformable model, we have succeeded in; (a) increasing the local flexibility of the surface by automatically adjusting the weights of the control points, (b) controlling the local shape with B-Spline basis functions and (c) automating surface initialisation. Experiments to determine the reliability of the proposed technique are carried out on MR head scans of 16 healthy subjects.

2. Initial Brain Segmentation

The purpose of this stage is to obtain an initial surface located close to the actual brain surface. This surface may not necessarily be the true brain surface but an approximation that will be deformed to conform to the actual boundary of the brain matter. At the beginning, the voxels of the original MR head scans (Fig. 1(a)) are converted to have isotropic dimensions of $1 \times 1 \times 1$ mm^3 to facilitate distance transformations. The scans are then filtered using an edge preserving 3D neighbourhood averaging routine [5]. The filtered

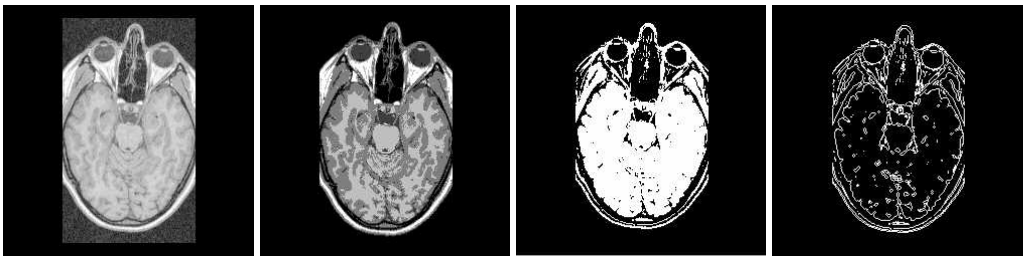

(a) (b) (c) (d)

(e) (f) (g)

Figure 1: Approximate initial segmentation of MR head scans: (a) original MR head scan, (b) intensity clustered image, (c) binary masking of gray and white matter, (d) boundary points of gray and white matter, (e) binary opening (f) binary closing of the largest connected component and (g) masking with the source image.

image is then clustered into five classes; cerebro-spinal fluid (CSF), gray matter (GM), white matter (WM), skull and background (Fig. 1(b)). Next, a binary mask containing GM and WM is generated (Fig. 1(c)). To open the narrow paths that links the brain with other external structures, border points of brain matter are extracted (Fig. 1(d)) and a 3D distance transformation [2] is applied to yield all the connected regions located outside 2 pixels from these boundary points resulting in a binary image (Fig. 1(e)). This distance is chosen based on the percentage of CSF found between the skull and the brain.

Other than the background region, the largest connected component in the distance-transformed binary image is the brain matter. A 3D binary closing [6] is applied to this component and this morphed image (Fig. 1(f)) is masked with the filtered MR source to obtain an approximate brain matter (Fig. 1(g)) that will be used to construct the initial NURBS surface.

2.1. Initial NURBS surface

The border points of the extracted brain, as shown in Fig. 2, form a continuous stream of voxels around the brain matter. From this representation, we sample a set of coordinate positions by rotating an axis about the centre of gravity of the boundary in each slice (the u and v directions are on the *x-y* plane and in the z direction, respectively). The intersecting points of this axis and the boundary give the control points of the NURBS surface. The angle of rotation of the axis at each sample determines the number of control points needed.

2.2. Energy Minimising Surface

The brain surface is a two-parameter vector-valued mathematical function $\mathbf{S} : [0,1] \times [0,1] \rightarrow \mathbb{R}^3$ such that an arbitrary point on the surface is parametrically expressed as $\mathbf{S}(u,v)$, $(u,v) \in [0,1]$. The internal energy E_{int} at a point $\mathbf{S}(u,v)$ on the brain surface $\mathbf{S}$ is defined as

$$E_{int}(\mathbf{S}(u,v)) = \frac{1}{2}\left(c_{10}\left|\frac{\partial \mathbf{S}(u,v)}{\partial u}\right|^2 + c_{01}\left|\frac{\partial \mathbf{S}(u,v)}{\partial v}\right|^2 \right.$$

$$\left. + c_{11}\left|\frac{\partial^2 \mathbf{S}(u,v)}{\partial u \partial v}\right|^2 + c_{20}\left|\frac{\partial^2 \mathbf{S}(u,v)}{\partial u^2}\right|^2 + c_{02}\left|\frac{\partial^2 \mathbf{S}(u,v)}{\partial v^2}\right|^2 \right) \quad (1)$$

where $c_{ij} \in \mathbb{R}$ [3]. The external energy E_{ext} at a point $\mathbf{S}(u,v)$ on the brain surface $\mathbf{S}$ is defined as

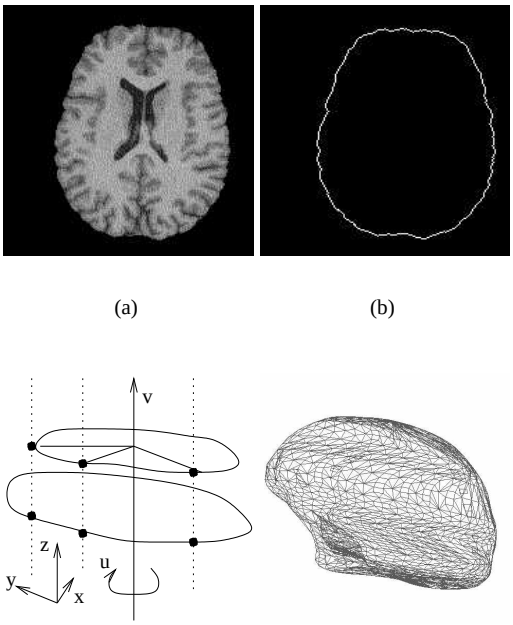

(a) (b) (c) (d)

Figure 2: Constructing the initial NURBS surface of the brain: (a) approximately segmented brain slice, (b) boundary of the brain, (c) extraction of the control points and (d) tessellated NURBS surface.

$$E_{ext}(\mathbf{S}(u,v)) = -\gamma \left|\nabla I(\mathbf{S}(u,v))\right|^2 \tag{2}$$

where $\gamma \in \mathbb{R}$ and $I(\mathbf{S}(u,v))$ gives the intensity of the image I at a point $\mathbf{S}(u,v)$. If $\mathbf{S}(u,v,t)$ denotes a surface $\mathbf{S}$ at time $t \in [0,\infty)$, an active brain surface at time $t+1$ is given by

$$\mathbf{S}(u,v,t+1) = \arg\min_{\mathbf{S}\in\mathcal{S}}(E(\mathbf{S}(u,v,t))) \tag{3}$$

where $\mathcal{S}$ represents all the possible surfaces at time t and

$$\begin{aligned} E(\mathbf{S}(u,v,t)) &= \iint_{(u,v)\in\mathbf{S}} (E_{int}(\mathbf{S}(u,v,t)) \\ &+ E_{ext}(\mathbf{S}(u,v,t)))\, dudv \end{aligned}$$

gives the total energy of $\mathbf{S}$ at time t.

2.3. NURBS-based Deformable Surface Model

Let $\mathbf{p}_{i,j}^t, i = 0,1,...,n-1, j = 0,1,...,m-1$ be the control points, having weights $w_{i,j}^t \in \mathbb{R}^+$, of an active NURBS surface $\mathbf{S}$, at time t, given by

$$\mathbf{S}(u,v,t) = \sum_{i=0}^{n-1}\sum_{j=0}^{m-1} R_{i,j}(u,v,t)\mathbf{p}_{i,j}^t \tag{4}$$

where

$$R_{i,j}(u,v,t) = \frac{w_{i,j}^t N_{i,p}(u) N_{j,q}(v)}{\sum_{c=0}^{n-1}\sum_{d=0}^{m-1} w_{c,d}^t N_{c,p}(u) N_{d,q}(v)}$$

are the rational basis functions in which $N_{l.k}$ gives the l^{th} B-Spline basis function of degree $k \in \mathbb{Z}^+$ such that

$$N_{l,0}(s) = \begin{cases} 1, & \text{if } s \in [s_l, s_{l+1}) \\ 0, & \text{otherwise} \end{cases}$$

and

$$N_{l,k}(s) = \frac{(s-s_l)N_{l,k-1}(s)}{s_{l+k}-s_l} + \frac{(s_{l+k+1}-s)N_{l+1,k-1}(s)}{s_{l+k+1}-s_{l+1}}$$

where s_l are positive real numbers referred to as *knots* [12].

2.4. Deformable NURBS Surface

The brain image in Fig. 1(g) does not exhibit the true 3D patterns of the brain surface because it contains low intensity CSF that fills sulci cavities. In the second stage of our technique, the approximate NURBS surface obtained previously is deformed so that it wraps itself onto the cavities and the hills on the brain surface. The NURBS surface given in Eq. (4) can also be expressed in matrix form as $\mathbf{S} = \mathbf{p}^{\mathrm{T}}\mathbf{R}$ where $\mathbf{p} = \left(\mathbf{p}_{0,0}^t, \mathbf{p}_{0,1}^t, ..., \mathbf{p}_{0,m-1}^t, \mathbf{p}_{1,0}^t, \mathbf{p}_{1,1}^t, ..., \mathbf{p}_{n-1,m-1}^t\right)^{\mathrm{T}}$ and $\mathbf{R} = \left(R_{0,0}, R_{0,1}, ..., R_{0,m-1}, R_{1,0}, ..., R_{n-1,m-1}\right)^{\mathrm{T}}$

Using Eq. (1), the total internal energy of the NURBS surface $\mathbf{S}$ is given by

$$E_{int}(\mathbf{S}) = 0.5\mathbf{p}^{\mathrm{T}}\mathbf{L}\mathbf{p} \tag{5}$$

where

$$\begin{aligned} \mathbf{L} &= \iint_{(u,v)\in\mathbf{S}} \left(c_{10}\mathbf{R}_u^{\mathrm{T}}\mathbf{R}_u + c_{01}\mathbf{R}_v^{\mathrm{T}}\mathbf{R}_v + c_{11}\mathbf{R}_{uv}^{\mathrm{T}}\mathbf{R}_{uv}\right. \\ &+ \left. c_{20}\mathbf{R}_{uu}^{\mathrm{T}}\mathbf{R}_{uu} + c_{02}\mathbf{R}_{vv}^{\mathrm{T}}\mathbf{R}_{vv}\right) dudv \end{aligned}$$

To compute the internal energy function in Eq. (5), the partial integrations of the rational basis functions $R_{i,j}$ have to be derived. Note that for the sake of simplicity, the degree

term k of the B-Spline basis functions will be omitted. We derive the first partial integrations of $R_{i,j}$ as:

$$R^u_{i,j}(u,v,t) = \frac{w^t_{i,j} N_j(v) \mathbf{N}_i(u) \mathbf{W} \mathbf{N}^{\mathrm{T}}(v)}{Q^2} \text{ and}$$

$$R^v_{i,j}(u,v,t) = \frac{w^t_{i,j} N_i(u) \mathbf{N}(u) \mathbf{W} \mathbf{N}^{-}_j(v)}{Q^2}$$

where $\mathbf{N}(\cdot) = (N_0(\cdot), N_1(\cdot), ..., N_{n-1}(\cdot))$, $\mathbf{N}_i(u) = N'_i(u)\mathbf{N}(u) - N_i(u)\mathbf{N}'(u)$, $\mathbf{N}^{-}_j(v) = N'_j(v)\mathbf{N}^{\mathrm{T}}(v) - N_j(v)\mathbf{N}^{\mathrm{T}'}(v)$, $N'_f(s) = \partial N_f(s)/\partial s; f \in (i,j), s \in (u,v)$, $\mathbf{W} = \left\{w^t_{i,j}\right\}_{n-1 \times m-1}$ and $Q = Q(u,v,t) = \Sigma\Sigma w^t_{i,j} N_i(u) N_j(v) = \mathbf{N}(u)\mathbf{W}\mathbf{N}^{\mathrm{T}}(v)$. Proceeding further, the second partial integrations are derived as:

$$R^{uu}_{i,j}(u,v,t) = \frac{w^t_{i,j} N_j(v) \left(Q\mathbf{N}'_i(u)\mathbf{X} - 2Q_u \mathbf{N}_i(u)\mathbf{X}\right)}{Q^3} \text{ and}$$

$$R^{vv}_{i,j}(u,v,t) = \frac{w^t_{i,j} N_i(u) \left(Q\mathbf{Y}\mathbf{N}^{-'}_j(v) - 2Q_v \mathbf{Y}\mathbf{N}^{-}_j(v)\right)}{Q^3}$$

where $\mathbf{X} = \mathbf{W}\mathbf{N}^{\mathrm{T}}(v)$ and $\mathbf{Y} = \mathbf{N}(u)\mathbf{W}$. Further,

$$R^{uv}_{i,j}(u,v,t) = \frac{w^t_{i,j} Q \mathbf{N}_i(u) \mathbf{W} \mathbf{N}^{+}_j(v) - 2N_j(v) Q_v \mathbf{N}_i(u)\mathbf{X}}{Q^3}$$

where $\mathbf{N}^{+}_j(v) = N_j(v)\mathbf{N}^{\mathrm{T}'}(v) + N'_j(v)\mathbf{N}^{\mathrm{T}}(v)$, $Q_u = \partial Q/\partial u$ and $Q_v = \partial Q/\partial v$. The above partial integrations are used to asses $\mathbf{R}_u, \mathbf{R}_v, \mathbf{R}_{uu}, \mathbf{R}_{vv}, \mathbf{R}_{uv}$ from $\mathbf{R}$.

The total external energy of $\mathbf{S}$, using Eq. (2), is given by $E_{ext}(\mathbf{S}) = -M$ where

$$M = \iint_{(u,v)\in\mathbf{S}} \gamma \left(I_u\left(\mathbf{p}^{\mathrm{T}}\mathbf{R}\right) + I_v\left(\mathbf{p}^{\mathrm{T}}\mathbf{R}\right)\right) du dv$$

with

$$I_s\left(\mathbf{p}^{\mathrm{T}}\mathbf{R}\right) = \left|\frac{\partial}{\partial s}\varphi \star I\left(\mathbf{p}^{\mathrm{T}}\mathbf{R}\right)\right|^2 ;\ s \in (u,v)$$

in which $\varphi\star$ denotes convolution with a Gaussian. Therefore, the total energy of the NURBS surface $\mathbf{S}$ is

$$E(\mathbf{S}) = \left(0.5\mathbf{p}^{\mathrm{T}}\mathbf{L}\mathbf{p} - M\right) \tag{6}$$

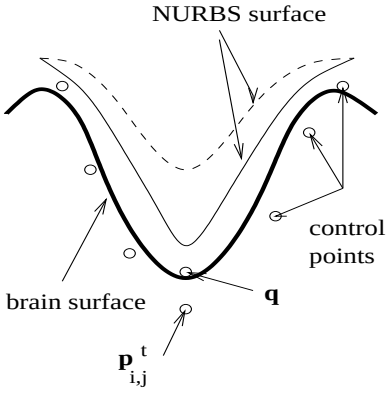

Figure 3: The NURBS surface is attracted toward the sulci cavity when the weight $w^t_{i,j}$ of the control point $\mathbf{p}^t_{i,j}$ is increased (dashed line indicates the surface location before weight adjustment).

The energy minimising process of a deformable surface, given in Eq. (3), is solved iteratively by considering the Euler-Lagrange equation $\nabla E(\mathbf{S}) = 0$. It gives a state of equilibrium to Eq. (6) from which the new locations of the control points in $\mathbf{p}$ are computed. Subsequently, a new NURBS surface is fitted over $\mathbf{p}$ whose local shape is further adjusted by modifying the weights of the control points as described next.

2.5. Weight Adjustment

When the deformable NURBS surface evolves through the energy minimising states, some segments may not be situated close to the actual brain matter. In such a case, the only way to move the surface towards these regions, without translating the control points, is by increasing the weight of the relevant control points [11]. Moreover, this weight modification must not effect parts of the surface located outside sulci cavities.

As shown in Fig. 3, let $\mathbf{q}$ be a point at the bottom of a sulci towards which the NURBS surface $\mathbf{S}$ needs to be attracted by adjusting the weight of the control point $\mathbf{p}^t_{i,j}$ (note that $\mathbf{q}$ is not a control point). If $\mathbf{S}$ is at $\mathbf{q}$ at time $t+1$, the NURBS form of the evolving surface becomes

$$\frac{\Sigma\Sigma w^{t+1}_{i,j} N_i(u) N_j(v) \mathbf{p}^t_{i,j}}{\Sigma\Sigma w^{t+1}_{i,j} N_i(u) N_j(v)} - \frac{\Sigma\Sigma w^t_{i,j} N_i(u) N_j(v) \mathbf{p}^t_{i,j}}{\Sigma\Sigma w^t_{i,j} N_i(u) N_j(v)}$$

$$= \mathbf{q} - \mathbf{S}(u,v,t) \tag{7}$$

Note that during weight adjustments, the position of a control point remains unchanged; i.e. $\mathbf{p}^{t+1}_{i,j} = \mathbf{p}^t_{i,j}$. If the weight change is denoted by $\Delta w^t_{i,j} = w^{t+1}_{i,j} - w^t_{i,j}$, Eq. (7) can be written as

$$
\begin{aligned}
&Q\left(\Sigma\Sigma w_{i,j}^{t} N_i(u) N_j(v) \mathbf{p}_{i,j}^{t} + \Sigma\Sigma \Delta w_{i,j}^{t} N_i(u) N_j(v) \mathbf{p}_{i,j}^{t}\right) \\
&-\Sigma\Sigma w_{i,j}^{t} N_i(u) N_j(v) \mathbf{p}_{i,j}^{t} \left(Q + \Sigma\Sigma \Delta w_{i,j}^{t} N_i(u) N_j(v)\right) \\
&= Q\left(Q + \Sigma\Sigma \Delta w_{i,j}^{t} N_i(u) N_j(v)\right)\left(\mathbf{q} - \mathbf{S}(u,v,t)\right)
\end{aligned} \tag{8}
$$

Multiplying Eq. (8) by $1/Q$ yields

$$
\begin{aligned}
&\sum_{i=0}^{n-1} \sum_{j=0}^{m-1} \Delta w_{i,j}^{t} N_i(u) N_j(v) \left(\mathbf{p}_{i,j}^{t} - \mathbf{q}\right) \\
&= \left(\mathbf{q} - \mathbf{S}(u,v,t)\right) Q(u,v,t)
\end{aligned} \tag{9}
$$

Now, Eq. (9) gives the weight changes $\Delta w_{i,j}^{t}$ to expand the deformable NURBS surface $\mathbf{S}$ towards the sulci cavity because it causes a perspective functional translation of the points on the effected NURBS segment toward $\mathbf{p}_{i,j}^{t}$.

Due to the continuous nature of the NURBS surface, an analytical solution for the curvature of the surface near the control point $\mathbf{p}_{i,j}^{t}$ is computed by taking the distance between $\mathbf{p}_{i,j}^{t}$ and the average vector $\mathbf{g}(\mathbf{p}_{i,j}^{t})$ of all the connected neighbouring control points of $\mathbf{p}_{i,j}^{t}$, denoted by $\mathcal{N}(\mathbf{p}_{i,j}^{t})$, which approximates the surface curvature at $\mathbf{p}_{i,j}^{t}$. The approximate surface curvature at $\mathbf{p}_{i,j}^{t}$, $\kappa_{i,j}^{t}$, is given by $\kappa_{i,j}^{t} = \left|\mathbf{p}_{i,j}^{t} - \mathbf{g}(\mathbf{p}_{i,j}^{t})\right|^2$ where

$$
\mathbf{g}(\mathbf{p}_{i,j}^{t}) = \frac{1}{\left\|\mathcal{N}(\mathbf{p}_{i,j}^{t})\right\|} \sum_{\mathbf{p}_{i',j'}^{t} \in \mathcal{N}(\mathbf{p}_{i,j}^{t})} \mathbf{p}_{i',j'}^{t}
$$

in which $\left\|\mathcal{N}(\mathbf{p}_{i,j}^{t})\right\|$ gives the number of control points in $\mathcal{N}(\mathbf{p}_{i,j}^{t})$. If the surface curvature $\kappa_{i,j}^{t}$ exceeds a threshold (say, the average surface curvature $= \frac{1}{n \times m} \Sigma\Sigma \kappa_{i,j}^{t}$), the weight $w_{i,j}^{t}$ is updated such that

$$
w_{i,j}^{t+1} = w_{i,j}^{t} + \eta \frac{\kappa_{i,j}^{t}}{\max_{i,j}\left\{\kappa_{i,j}^{t}\right\}}
$$

where $\eta \in \mathbb{R}$ controls the amount of attraction of the surface towards the control point. This local shape control of the surface, due to weight adjustments, comes from the B-Spline basis functions where $N_{l,k}(s) = 0$ for $s \notin [s_l, s_{l+k+1})$. The knots for the two B-Spline basis functions $N_{i,p}(u)$ and $N_{j,q}(v)$ are given by the vectors $(u_0, u_1, ..., u_{n+p})^{\mathrm{T}}$ and $(v_0, v_1, ..., v_{m+q})^{\mathrm{T}}$, respectively. Each knot pair (u_i, v_j) relates the parameters u and v to a weight $w_{i,j}^{t}$ such that an adjustment of $w_{i,j}^{t}$ affects only the surface segment $\mathbf{S}(u,v,t)$, $(u,v) \in [u_i, u_{i+p+1}) \times [v_j, v_{j+q+1})$ [12]. Finally, the brain matter is extracted after removing all the voxels situated outside the deformed NURBS surface.

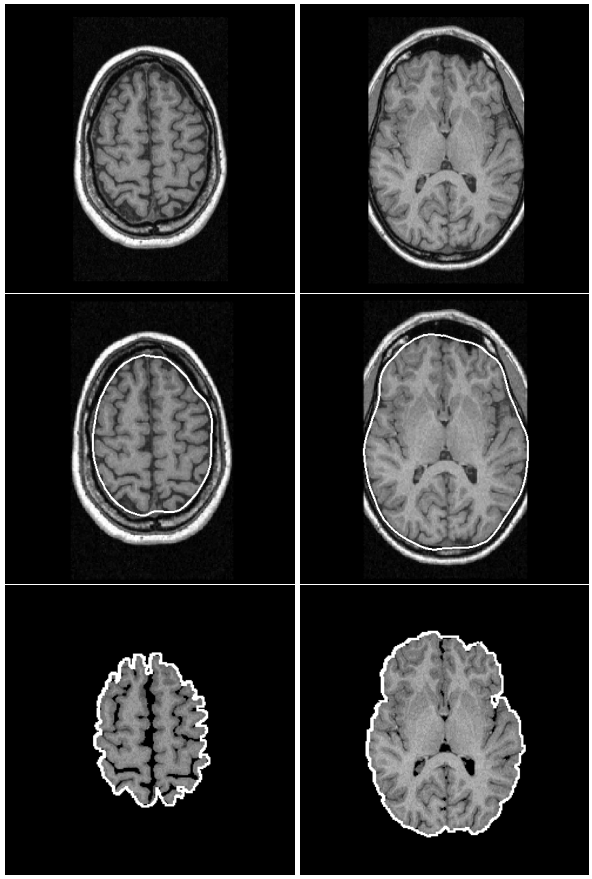

Figure 4: MR image slices of the brain: (top) original MR images, (middle) NURBS surface initialised close to the brain and (bottom) brain slices segmented with NURBS-based deformable surface.

3. Results

To validate the preciseness of the proposed technique, 16 MR head scans of healthy volunteers, between the ages of 6 and 27, were processed. The actual boundary of the brain surface was extracted by manually outlining the outer perimeter of the brain matter of each slice.

Fig. 4 depicts segmented results of an MR head scan. Although our algorithm is implemented in 3D, the images are shown as 2D slices for enhanced clarity. The accuracy and the shape difference of the NURBS-based and manual segmentation was measured using the average distance error between the two surfaces [16]. It is the average distance between each point on the deformed NURBS surface $\mathbf{S}$ and the closest point on the actual brain surface $\widehat{\mathbf{S}}$. The average distance error ,*e*, is given by

$$
e(\mathbf{S}, \widehat{\mathbf{S}}) = \frac{1}{A} \iint_{(u,v) \in \mathbf{S}} \min_{(u',v') \in \widehat{\mathbf{S}}} \left|\mathbf{S}(u,v) - \widehat{\mathbf{S}}(u',v')\right| du dv
$$

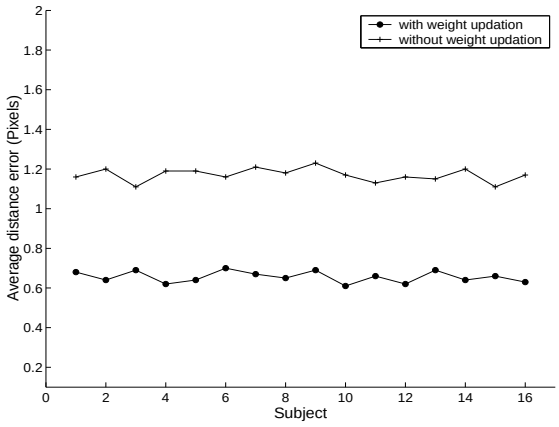

Figure 5: Performance measurement of the proposed technique on 3D MR images using the average distance error.

where A is the surface area of $\mathbf{S}$. It can be observed in Fig. 5, where the X-axis gives the subject number (i.e. the volunteer's MR head scan number), that the error is below 1 pixel in all the cases when the weights $w_{i,j}^t$ are updated; the lowest being 0.60 pixels and the highest error being 0.71 pixels. When the weights are not updated, the lowest and the highest errors are 1.11 and 1.23 pixels, respectively. In other words, the brain, segmented using the NURBS framework with weight adjustments, is situated closer to the true brain surface than the segmentation obtained without weight adjustments for the same number of iterations. These results match with increased performance over those reported by other investigators [4, 17]. When the weights are not updated, the deformable model behaves as a B-Spline surface that does not exhibit rational properties to give an extra degree of freedom for shaping the surface. The process takes, on the average, 10 minutes to peel a 3D volumetric image in a Sun Sparc 60 workstation.

4. Conclusion

A new technique based on NURBS to segment the brain from MR head scans is presented. The deformable NURBS surface exploits the weighting parameter at each control point that is updated automatically to detect sharp cavities found on the brain surface. Moreover, the model does not contain an initialisation problem because the initial NURBS surface is formed automatically using an approximate brain segmentation routine. It guarantees that the surface initialisation is close to the actual brain matter and thus, avoids the evolving surface getting stuck in a local minima. The current approach, which integrates image processing, computer graphics and vision, provides clinicians an accurate tool to carry out surface-based structural analysis of the human brain and other visualisation tasks in neuroimaging studies.

References

[1] S. Atkins and B. Mackiewich. Fully automated segmentation of the brain in MRI. *IEEE Trans. Medical Imaging*, 17(1):99–107, 1998.

[2] G. Borgefors. Distance transformation in arbitrary dimensions. *Computer Vision, Graphics and Image Processing*, 27:321–345, 1986.

[3] I. Cohen, L. Cohen, and N. Ayache. Using deformable surfaces to segment 3D images and infer differential structures. *Computer Vision, Graphics and Image Processing:Image Understanding*, 56(2):242–263, 1992.

[4] C. Davatzikos and R. Bryan. Using a deformable surface model to obtain a shape representation of the cortex. *IEEE Trans. Medical Imaging*, 15(6):785–795, 1996.

[5] F. Kruggel and D. von Cramon. Alignment of magnetic resonance brain datasets with the stereotactical coordinate system. *Medical Image Analysis*, 3(2):175–185, 1999.

[6] P. Maragos and R. Schafer. Morphological systems for multidimensional signal processing. In *Proc. IEEE*, volume 78, pages 690–719, 1990.

[7] T. McInerny and D. Terzopoulos. Deformable models in medical image analysis. In *Proc. Workshop on Mathematical Methods in Biomedical Image Analysis*, pages 171–180, 1996.

[8] T. McInerny and D. Terzopoulos. Topology adaptive deformable surface for medical image volume segmentation. *IEEE Trans. Medical Imaging*, 18(10):840–850, 1999.

[9] W. Niessen, K. Vincken, J. Weickert, and M. Viergever. Three-dimensional MR brain segmentation. In *Proc. 6th Int. Conf. on Computer Vision (ICCV'98)*, pages 53–58, 1998.

[10] M. Ono and S. Kubik. *Atlas of the cerebral sulci*. George-Thieme Verlag, Stuttgart, 1990.

[11] L. Piegl. Modifying the shape of rational B-splines. Part 2:Surfaces. *Computer Aided Design*, 21(9):538–546, 1989.

[12] L. Piegl and W. Tiller. *The NURBS Book*. Springer-Verlag, 1995.

[13] H. Qin and D. Terzopoulos. D-NURBS: A physics-based framework for geometric design. *IEEE Trans. Visualization and Computer Graphics*, 2(1):85–95, 1996.

[14] S. Sandor and R. Leahy. Surface-based labeling of cortical anatomy using a deformable atlas. *IEEE Trans. Medical Imaging*, 16(1):41–54, 1997.

[15] J. Snell, M. Merickel, J. Ortega, J. Gobel, J. Brookman, and N. Kassel. Model based boundary estimation of complex objects using hierarchical active surface template. *Pattern Recognition*, 28(10):1599–1609, 1995.

[16] L. Staib and J. Duncan. Model-based deformable surface finding for medical images. *IEEE Trans. Medical Imaging*, 15(6):859–870, 1996.

[17] C. Xu, D. Pham, M. Rettmann, D. Yu, and J. Prince. Reconstruction of the human cerebral cortex from magnetic resonance images. *IEEE Trans. Medical Imaging*, 18(6):467–480, 1999.